Single view single light multispectral object segmentation

Eduard Schick
TU Dortmund University
Image Analysis Group
Otto-Hahn-Straße 4
44227, Dortmund,
Germany
eduard.schick@tu-dortmund.de

Steffen Herbort
TU Dortmund University
Image Analysis Group
Otto-Hahn-Straße 4
44227, Dortmund,
Germany
steffen.herbort@tu-dortmund.de

Arne Grumpe
TU Dortmund University
Image Analysis Group
Otto-Hahn-Straße 4
44227, Dortmund,
Germany
arne.grumpe@tu-dortmund.de

Christian Wöhler
TU Dortmund University
Image Analysis Group
Otto-Hahn-Straße 4
44227, Dortmund,
Germany
christian.woehler@tu-dortmund.de

ABSTRACT

In this paper we present an approach for the acquisition and segmentation of spectral Bidirectional Reflectance Distribution Function (BRDF) measurements of real-world objects. The acquisition setup is a priori fully calibrated and provides pixel-synchronous image and depth data of the examined objects. Based on one single viewing and illumination geometry, we are able to determine spectrally distinct surface regions for objects with abruptly changing surface materials (painted surface patches) and for objects with gradually changing materials (partially oxidized iron). For clustering we apply the *k*-means algorithm and the mean-shift algorithm. The segmented clusters are used to adapt individual spectral BRDFs (Lambert, Phong, Cook-Torrance) to the obtained cluster data. Additionally, the elemental abundances of iron and rust on a metal surface are analyzed using spectral unmixing. The paper presents a detailed discussion of our method and provides critical insight into the obtained results.

Keywords

multispectral data, segmentation, *k*-means, mean-shift, BRDF, linear unmixing

1 INTRODUCTION

The amount of light perceived from a point on an arbitrary illuminated object surface depends on the type and direction of the incident light, the surface geometry, the scene geometry, and, especially, on the object material at any given point. Industrial applications show that it is desirable to develop methods for the determination of regions with common or distinct spectral reflectance behavior. The knowledge of local material properties can then be used for e.g. material identification or image based surface reconstruction [HB86, Woo80, HW12]. While successful material separation has been presented by different researchers (e.g. [Tom02, NRN03, LKG$^+$03]), their data acquisition involved a varying light source position and a varying camera position, which requires an intricate measurement scenario involving a high effort for data acquisition.

In this paper, we present a method for the separation of material components based on their multispectral reflectance characteristics using a static object, a single light source position, and a fixed camera position. For industrial applications, it is desirable to use as few light and camera positions as possible, since this facilitates the acquisition process and reduces the required recording time. However, this comes at the cost of the measurements covering only a small range of possible angles of observance ($\vartheta_o \in [-90^\circ ... +90\,^\circ] \subset \mathbb{R}$) and incidence ($\vartheta_i \in [-90^\circ ... +90^\circ] \subset \mathbb{R}$). While it is challenging to cluster and/or perform model fits using that data basis, we will show that it is possible if the underlying models are modified. We are thus able to obtain correct segmentations for almost the whole object, even though there is no wide range of illumination and viewing angles available due to the single view single light configuration.

We compare the application of different clustering approaches (*k*-means clustering and mean-shift clustering) for the examination of a surface with sharp material changes (color patches), and for a surface with smooth material changes (iron vs. iron oxide). For the segmentation, it is physically impossible to cluster the data based on specular reflections, since these only depend on the color of the incident light and are independent of the surface color as explained in detail by [Sha85]. The segmentation can thus be performed on the diffuse part only. We show that it is possible to improve the segmentation results considerably by an empirical modification of the modeled reflectance behavior.

In the subsequent stage we use each cluster to obtain the parameters of a model-based spectral BRDF[1], and we compare the performance of the Phong [Pho75] and Cook-Torrance [CT81] models. Additionally, we show

[1] Bidirectional Reflectance Distribution Function

 ISBN 978-80-86943-74-9

that the clustered data can be used to determine the abundance distribution of – in our case – iron and iron oxide using linear unmixing without any adjustment of the underlying BRDF.

2 RELATED WORK

The problem of separating material from shape and illumination has been examined by some authors previously. However, most of them use some sort of varying light source position and/or varying viewpoint.

[Tom02] applies multispectral data to the problem of circuit board element segmentation. Initially, two images are recorded with different illumination directions, which are used for a very coarse initial segmentation and measurements that contain specular reflections are removed. The remaining pixels are clustered based on a set of empirically defined if-then-else classification rules, which emerge from a priori knowledge of the spectral reflectance properties of the circuit board elements. In summary, [Tom02] operate on the diffuse part only, require different illumination directions, and rely on a priori knowledge for the clustering process.

[NRN03] present "photometric invariants", which can be used for various tasks, including material segmentation. In detail, they aim for a separation of material from lighting and shape based on a scene description with separable BRDFs. The availability of multispectral data (color images) under different illumination conditions then allows for solving for a geometric invariant by simply computing ratios of matrix determinants. The authors show successful application of their method to isolated homogeneous objects, homogeneous objects in complex environments, objects consisting of different materials, inhomogeneous objects, and objects with a specular surface. However, the invariants require changes in illumination, viewpoint, and/or object position between consecutive acquisitions.

[LKG+03] acquire geometric and photometric data using different light source positions and viewpoints for a set of "lumitexels", which are assembled as a vector of geometric and photometric measurements. Afterwards, they fit the Lafortune BRDF model to all lumitexels to create two BRDF models along with a covariance matrix of the fitting parameters. Based on the error between lumitexels and those two BRDFs, they split the surface consecutively into two clusters. This procedure is repeated for the cluster with the greatest deviation of measured and fitted BRDF until a clear segmentation of all material components is achieved.

3 CONTRIBUTION

We present a novel method for the segmentation of multispectral data. In contrast to [LKG+03] and [NRN03], we apply a fixed object, light source, and camera position. Unlike [Tom02], we do not require any prior knowledge of the material reflectance. Fig. 1 shows an image of the experimental setup and Fig. 2 gives an overview of our algorithm. Initially, we record

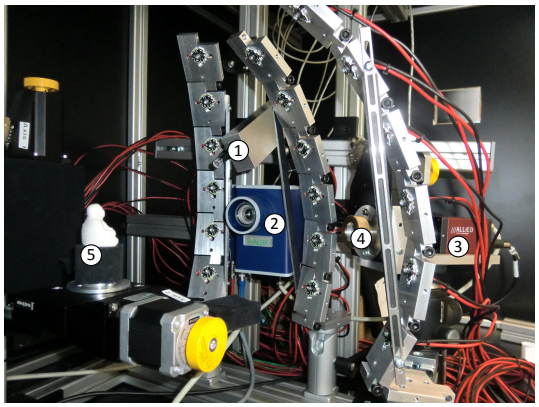

Figure 1: Experimental setup including light source (1), camera (3), 3D scanner (2+3) and interference bandpass filters (4) for acquisition of the object data (5).

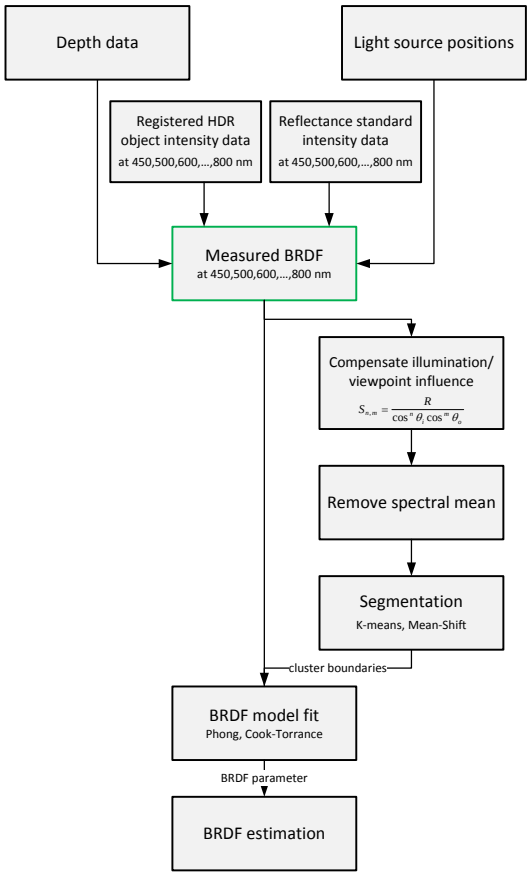

Figure 2: Methodical overview.

the depth data with a 3D laser pattern projector[2] and acquire image data for $N = 8$ distinct wavelengths

[2] ViALUX zSnapper Vario, 2048 $px \times 2048\,px$, lateral resolution $\approx 40\,\mu$m

 ISBN 978-80-86943-74-9

between 450 and 800 nm) using bandpass interference filters[3]. The light source positions and intensities are known a priori following the calibration procedure described by [LHW12]. Additionally, the image data of a white diffuse reflectance standard[4] is recorded, which is later used to infer the BRDF from the observed intensity data (Section 4).
Afterwards, compensate the influence of the incident and viewing directions is compensated, the spectral mean is removed, and the k-means and/or mean-shift algorithms are employed for clustering. With the clustering boundaries available, we are able to obtain BRDF parameters for each cluster and each multispectral channel within these clusters. Algorithmic details for these stages are explained in the following section.

4 ALGORITHMIC DETAILS

4.1 Data preparation

In order to account for even slight camera shifts during bandpass filter replacements or by the optically active bandpass filters themselves, we conduct an image registration and subsequent affine transformation step to account for these distortions. The dynamic range of the images is increased by using high dynamic range imaging (HDR), which allows capturing bright specular regions and dark surface regions without reaching saturation or losing low-contrasted details in the camera noise.
Since the depth data are corrupted by a considerable amount of noise, we perform a model-based fit to the acquired data. The models are chosen to simply match the object shape, i.e. a cylindrical model for the "cup" dataset and a plate for the "triangle" dataset (see Fig. 3 and Fig. 10). This is achieved by a minimization of the mean squared distance between the measured data points and the model surface. A whole description of that process lies beyond the focus of this paper and is therefore omitted, a detailed description can be found e.g. in [LMM98, Ebe08]. Note, that the multispectral data segmentation algorithm below is not restricted to the application of these models. The models only account for the partially severe amount of noise present in our 3D scans. The model fitting step is unnecessary, if the scanned surface contains only low noise.

4.2 BRDF measurement

The main idea for BRDF measurement determination lies in acquiring multispectral object and reflectance standard data, which are then related to each other as explained in the following. This derivation thus aims for an expression of the observed BRDF values f_r. The measured object intensity can be expressed as

$$I_{ob} = C \cdot \frac{I_0}{r_{l,ob}^2 r_{c,ob}^2} \cdot f_{r,ob} \cdot \cos\vartheta_{i,ob}, \tag{1}$$

where the distance from the light source to the object and the camera to the object are denoted $r_{l,ob}$ and $r_{c,ob}$, respectively. The light source intensity is I_0, the BRDF is $f_{r,ob}$. Further influencing quantities like camera gain or interference filter attenuation are all contained within the constant C. $\vartheta_{i,ob}$ denotes the angle of light incidence on the object surface, i.e. the angle between the local direction $\mathbf{l}$ of the incident light and the local normal vector $\mathbf{n}_{ob}$ of the surface such that $\cos\vartheta_{i,ob} = \langle \mathbf{l} \cdot \mathbf{n}_{ob} \rangle$.
Analogously, the reflectance standard is described by

$$I_{re}(x_0, y_0) = C \cdot \frac{I_0}{r_{l,re}^2 r_{c,re}^2} \cdot f_{r,re} \cdot \cos[\vartheta_{i,re}(x_0, y_0)] \tag{2}$$

In contrast to Eq. (1), we can include more prior knowledge here. For the reflectance standard, we can specify an approximately diffuse reflectance behavior and an a priori known spectral albedo $\rho_{re} = 0.99$ specified by the manufacturer. We thus replace the general BRDF $f_{r,re}$ by a Lambertian reflectance term, i.e. $f_{r,re} = \frac{\rho_{re}}{\pi}$, yielding

$$I_{re}(x_0, y_0) = C \cdot \frac{I_0}{r_{l,re}^2 r_{c,re}^2} \cdot \frac{\rho_{re}}{\pi} \cdot \cos[\vartheta_{i,re}(x_0, y_0)]. \tag{3}$$

Dividing Eq. (1) by Eq. (3) then leads to

$$f_{r,ob} = \frac{I_{ob}}{I_{re}} \cdot \frac{\rho_{re}}{\pi} \frac{\cos\vartheta_{i,re}(x_0, y_0)}{\cos\vartheta_{i,ob}} \cdot \frac{r_{l,ob}^2 r_{c,ob}^2}{r_{l,re}^2 r_{c,re}^2}, \tag{4}$$

which is connected to the reflectance R_{ob} by

$$f_{r,ob} = R_{ob} \cdot \frac{1}{\cos(\vartheta_{i,ob})}. \tag{5}$$

It is apparent that the relation of measured object intensities with reflectance standard data provides an elegant way for BRDF measurement determination. The BRDF obtained from Eq. (4) can now be used to segment areas based on their spectral reflectance. Ideally, the separated areas correspond to areas with the same material characteristics. Practically, a specular reflection within the surface leads to incorrect segmentation results. Due to the lack of varying light source or viewpoint position, a precise estimation of these illumination effects can not be achieved. Instead, we modify the measured reflectance samples R_{ob} (or, respectively, measured BRDF f_r) such that

$$S_{n,m} = \frac{R_{ob}}{\cos^n\vartheta_i \cos^m\vartheta_o} = \frac{f_r}{\cos^{n+1}\vartheta_i \cos^m\vartheta_o}, \tag{6}$$

[3] Thorlabs bandpass intereference filters, center wave length CWL = $[450, 500, 550, 600, 650, 700, 750, 800]\,nm$, full width at half maximum FWHM = $10\,nm$

[4] SphereOptics Zenith Polymer Diffuse Reflectance Standard SG3052

 ISBN 978-80-86943-74-9

which has been found to alleviate that effect. The angles $\vartheta_i = \arccos(\langle \mathbf{l} \cdot \mathbf{n} \rangle)$ and $\vartheta_o = \arccos(\langle \mathbf{v} \cdot \mathbf{n} \rangle)$ denote the angles between incident light direction $\mathbf{l}$ and observance direction $\mathbf{v}$ with the local surface normal $\mathbf{n}$, respectively. Additionally, we apply a spectral mean subtraction to Eq. (6) prior to segmentation since this has been found to improve the segmentation results (see Section 5) because it stresses the spectral gradient in comparison to the spectral offset.

4.3 Clustering and BRDF fitting

For clustering similar BRDF measurements, we use the k-means algorithm [Mar09] and the mean-shift algorithm [CM02] in their classical form, i.e. without functional adaptations. For the mean-shift algorithm, we apply a disk-shaped kernel that evenly weights the involved measurements [Fin06]. Once the clusters are obtained, we estimate a Phong [Pho75] and a Cook-Torrance [CT81] BRDF by nonlinearly fitting the $u = [1...U] \subset \mathbb{N}$ observed measurements $f_{r,u}^{observed}$ to the corresponding model based estimations $f_{r,u}^{modeled}$ such that

$$P^* = \underset{P}{\operatorname{argmin}} \sum_{u=1}^{U} (f_{r,u}^{observed} - f_{r,u}^{modeled})^2 \tag{7}$$

becomes minimized with respect to the model parameters P. Both BRDF models include a Lambertian term $\frac{k_d}{\pi}$ to describe (ideal) diffuse reflection. The applied physically plausible Phong BRDF is

$$f_r = \frac{k_d}{\pi} + k_s \frac{a+2}{2\pi} \underbrace{\langle \mathbf{r} \cdot \mathbf{v} \rangle^a}_{\cos^a \vartheta_{rv}}, \tag{8}$$

where a denotes an exponential coefficient for varying the angular extent of the specular component. The specular characteristics are modeled based on the angle ϑ_{rv} between the direction of mirror reflection $\mathbf{r}$ and observation $\mathbf{v}$.

The Cook-Torrance BRDF model consists the following terms:

$$f_r = k_d \frac{1}{\pi} + k_s \frac{F(n)}{\pi} \frac{D(m) \cdot G}{\cos \vartheta_i \cos \vartheta_o}. \tag{9}$$

The amount of reflected light depends of the three components F, D, and G, which denote the Fresnel reflection coefficient, the distribution function of the directions of the microfacets, and the geometrical attenuation factor, respectively. F improves the model exactness for grazing incidence angles, D defines the influence of surface roughness on lobe width, and G accounts for self shadowing and occlusion. The parameters of the Cook-Torrance BRDF are the weights k_d and k_s, the index of refraction n and the surface roughness m. Details can be obtained from [CT81].

4.4 Spectral unmixing

Spectral unmixing denotes the decomposition of the spectrum of a compound material into the spectra of the known pure materials out of which it consists by estimating the corresponding relative frequencies [KM02]. To estimate a distribution of a compound of two materials ("endmembers") – in our case: iron and iron oxide (rust), see Fig. 10(a) – we use a linear unmixing approach [KM02] such that the pixel-wise spectral BRDF $\mathbf{f_r} = [f_{r,1}, ..., f_{r,N}]^T \in \mathbb{R}^{N \times 1}$ sampled at N distinct wavelengths is supposed to be composed of two components $\mathbf{x}_{\text{iron}} \in \mathbb{R}^{N \times 1}$ and $\mathbf{x}_{\text{rust}} \in \mathbb{R}^{N \times 1}$ according to

$$\mathbf{x}_{\text{iron}} + \mathbf{x}_{\text{rust}} = \mathbf{BRDF} = \mathbf{f_r}. \tag{10}$$

These $\mathbf{x}$, in turn, are weighted variants of the spectral BRDFs of the pure elements ($\mathbf{r}_{\text{iron}}$ and $\mathbf{r}_{\text{rust}}$):

$$\mathbf{x}_{\text{iron}} = a_{\text{iron}} \cdot \mathbf{r}_{\text{iron}} \qquad \mathbf{x}_{\text{rust}} = a_{\text{rust}} \cdot \mathbf{r}_{\text{rust}}. \tag{11}$$

The vectors $\mathbf{r}_{\text{iron}}$ and $\mathbf{r}_{\text{rust}}$ represent reference spectra of iron and rust, which have been determined by averaging $K \in \mathbb{N}$ manually chosen BRDF samples $r_{iron,k}$ and $r_{rust,k}$ with $k = 1...K$ from the image:

$$\mathbf{r}_{\text{iron}} = \frac{1}{K} \sum_{k=1}^{K} \mathbf{r}_{iron,k}, \quad \mathbf{r}_{\text{rust}} = \frac{1}{K} \sum_{k=1}^{K} \mathbf{r}_{rust,k}. \tag{12}$$

This approach corresponds to the concept of image-based endmember selection [KM02]. To estimate the actual abundance distribution $a_{\text{iron}} \in [0...1] \subset \mathbb{R}$ and $a_{\text{rust}} \in [0...1] \subset \mathbb{R}$, we apply the following least-square transformation of Eq. (11):

$$a_{\text{iron}} = (\mathbf{r}_{\text{iron}}^T \mathbf{r}_{\text{iron}})^{-1} \mathbf{r}_{\text{iron}}^T \mathbf{x}_{\text{iron}} \tag{13}$$

$$a_{\text{rust}} = (\mathbf{r}_{\text{rust}}^T \mathbf{r}_{\text{rust}})^{-1} \mathbf{r}_{\text{rust}}^T \mathbf{x}_{\text{rust}} \tag{14}$$

For this to be physical meaningful, the following two constraints have to be satisfied:

$$a_{\text{iron}}(i) > 0,\ a_{\text{rust}}(i) > 0 \tag{15}$$

$$a_{\text{iron}}(i) + a_{\text{rust}}(i) = 1 \tag{16}$$

These constraints are added to Eq. (13) and Eq. (14) [KM02], which are then solved accordingly. Note that this derivation can be applied to the separation of two arbitrary materials with known or measured pure material BRDFs $\mathbf{r}_{\text{Material 1}}$ and $\mathbf{r}_{\text{Material 2}}$. In that case, the BRDF vectors $\mathbf{r}_{iron}$ and $\mathbf{r}_{rust}$ are replaced by the new BRDF vectors in the derivation above. The linear unmixing approach is also applicable to $N \in \mathbb{N} > 2$ material components.

5 EXPERIMENTS AND RESULTS

The following sections provide a detailed discussion of the "cup" dataset, which contains sharp boundaries (see Section 5.1), and of the "triangle" dataset, which exhibits a gradual transition between iron and iron oxide (see Section 5.2).

 ISBN 978-80-86943-74-9

5.1 Object with sharp region boundaries

The first part of this work deals with the segmentation of a dataset with abruptly changing regions on the surface of a cup as shown in Fig. 3(a). To compare segmentation results quantitatively, we manually created a reference cluster map, which is shown in Fig. 3(b). With that being available as a ground truth, the detection rate D is defined to be

$$D = \frac{\text{tp}}{\text{all}} \cdot 100\%, \tag{17}$$

i.e. the percentage of correctly classified pixels (tp) within the whole set of classifiable pixels in the image (all).

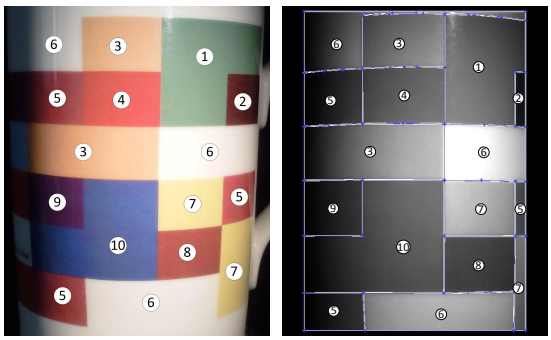

(a) Color regions of the examined cup (b) Manually defined reference clusters

Figure 3: Detection rate ground truth

Fig. 4 illustrates the pixel-wise detection rate for k-means and mean-shift for a varying number of clusters, bandwidth, and BRDF modification factor $S_{n,m}$, as described in Eq. (6). The red curve is equivalent to a direct BRDF segmentation (spectral mean free) without any BRDF modification. Both segmentation algorithms, especially mean-shift, benefit from the reflection model modification.

A detailed image of the best segmentation result yielded by mean-shift using $S_{1.6,0.5}$ is shown in Fig. 5. The segmentation error in the lower left part of the cup can be attributed to slightly overexposed input data originating from spurious illumination from interreflections with the experimental environment. The correct separation of the three reddish regions 4, 5 and 8 (see Fig. 4(a)) is especially challenging, due to the fact that the corresponding spectra are very similar and need to be distinguished based on merely 8 spectral measurements. Additionally, an oversegmentation of the orange cluster ③ can be observed. A toleration of the oversegmentation leads to a segmentation result with a detection rate of $D \approx 95\%$ as shown in Fig. 5(c) and Fig. 5(d). Note that the segmentation is correct over nearly the whole cup, i.e. even regions with steep surface gradients (cup borders), whose measurements are typically hard to obtain due to rapidly changing incidence and viewing angles, have been segmented correctly.

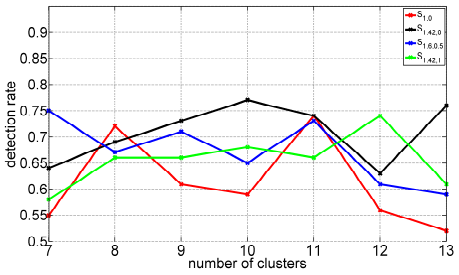

(a) k-means detection rate over number of clusters

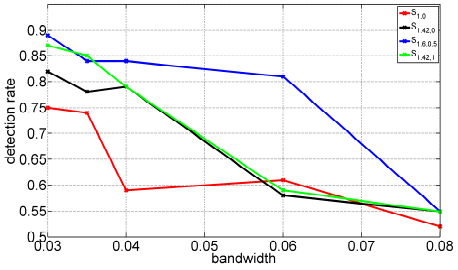

(b) mean-shift detection rate over bandwidth

Figure 4: Comparison of the correct segmentation rate between k-means and mean-shift for abrupt cluster transitions. Each curve (red, black, blue, green) corresponds to a different BRDF modification factor S.

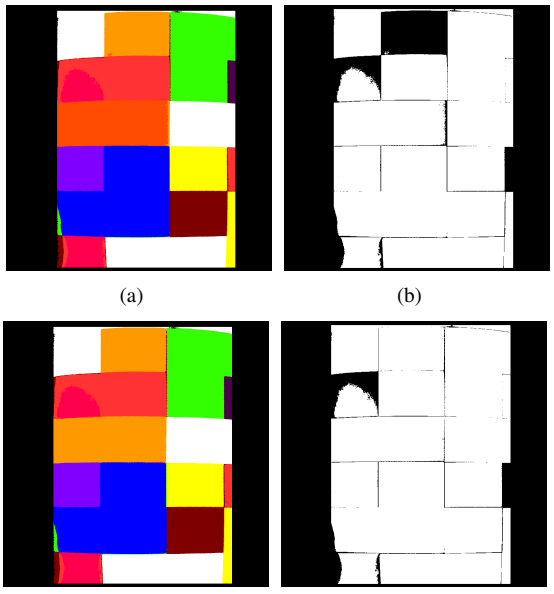

(a) (b) (c) (d)

Figure 5: Segmentation result for $S_{1.6,0.5}$. (a) Best mean-shift segmentation result without further treatment. (b) Correct detected areas (detection rate: 88.45 %). (c) Best mean-shift segmentation result with toleration of the oversegmented orange cluster. (d) Correct detected areas (detection rate: 94.79 %). Note the oversegmentation of the orange cluster ((a) and (b)), which can be neglected ((c) and (d)). Note that areas at the border of the cup with steep surface gradients have been segmented correctly.

The measured BRDF can now be approximated by a Phong and/or a Cook-Torrance BRDF model for each

 ISBN 978-80-86943-74-9

determined segmented cluster. Using the obtained BRDF parameters allows for a determination of a BRDF value for every half polar observation angle $\vartheta_o \in [-90°, ..., 90°] \subset \mathbb{R}$, for each incident light angle $\vartheta_i \in [-90°, ..., 90°] \subset \mathbb{R}$, and for each pixel belonging to the cluster. In our case, we analyze a pixel of a BRDF at 600 *nm* wavelength, which is located closely to a specular highlight. This pixel corresponds to cluster ①, which is generated by a mean-shift clustering of $S_{1.42,1}$ and visualized in Fig. 6(a) and Fig. 6(b).

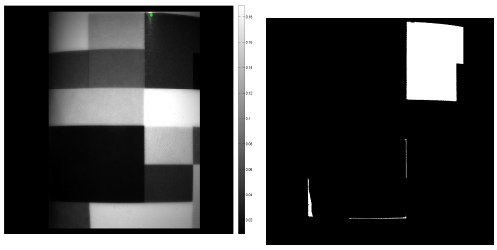

(a) (b)

Figure 6: Data point and corresponding clusters. (a) Measured BRDF at a wavelength of 600 *nm*. Observed point near measured specular maximum is marked green. (b) Segmented cluster including observed data point (mean-shift approach with $S_{1.42,1}$).

Fig. 7, Fig. 8 and Fig. 9 show the results of BRDF estimation for the Phong model (single lobe as well as lobe+spike variant) and the Cook-Torrance model (lobe+spike). Note that the range of incidence and viewing angles available for BRDF estimation is narrow but the estimation is robust due to the large number of pixels involved. The obtained BRDF may become inaccurate for angles a long way off from the underlying samples used during the parameter estimation stage, but model usage far off the data basis should be avoided anyway.

An important observation is that the BRDF decreases for large absolute viewing angles $|\vartheta_o| \geq 60°$. This effect has also been observed with other objects and scene settings. Relating this effect to the varying specular part of reflection does not seem very realistic due the fact that this decrease occurs at angles far away from the ideal specular reflection angle $\vartheta_{rv} = 0°$. In fact, a non-ideal diffuse reflection for grazing viewing angles is a more plausible explanation. [ON94] introduce a more detailed and complex diffuse reflectance term, but they describe an increased reflectance, which is contrary to our observations. The reflectance in this work better corresponds with a "diffuse fall-off" described e.g. by [DRS08]. This effect models decreasing reflectance for larger angles of observance and is partially taken into account by [LFTG97].

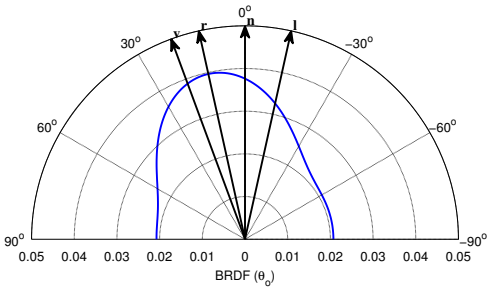

Figure 7: Phong fit (lobe).

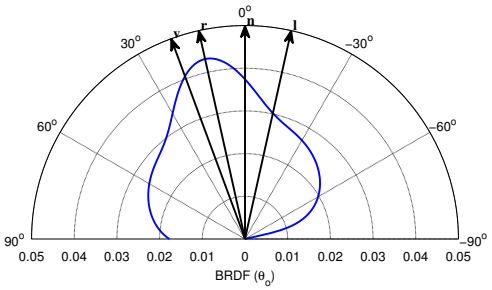

Figure 8: Phong fit (lobe+spike).

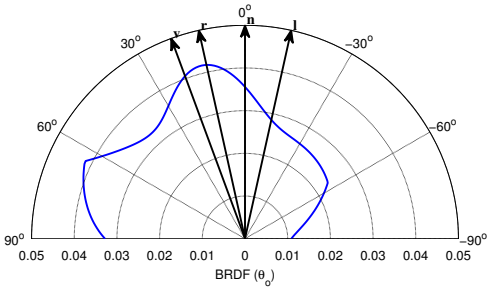

Figure 9: Cook-Torrance fit (lobe+spike).

5.2 Object with gradual region boundaries

Initially, we performed a *k*-means segmentation (see Fig. 10) of the oxidized iron object without any modifications of the BRDF, i.e. we used $S_{(1,1)}$. To obtain a robust segmentation result without the influence of spurious effects like specular reflections and other illumination inhomogeneities, we have chosen a planar arrangement of the object with high values of the specular angle ϑ_{rv} in order to minimize the occurrence of specular reflections. However, due to the roughness of the surface there is an inevitable amount of small surface parts that reflect light specularly into the camera. These have been taken into account by a *k*-means segmentation with 3 clusters, i.e. iron, oxidized iron, and a "garbage" class that collects outliers. Based on 10 manually chosen reference data points for iron and rust (as required for the linear unmixing approach described in Section 4.4), an abundance distribution of both materials can be estimated as shown in Fig. 11(a) and Fig. 11(b). On the basis of this distribution and an

 ISBN 978-80-86943-74-9

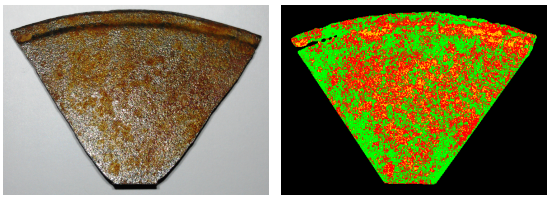

(a) Probed oxidized iron object. (b) Segmentation with k-means (3 clusters).

Figure 10: Visual comparison between original and segmented clusters. A third class ("garbage class") besides iron and rust has been introduced to collect outliers.

image registration approach that relates the color image Fig. 10(a) with the measurement data Fig. 11(a) and Fig. 11(b), a mask of the two materials can be generated as shown in Fig. 11(c) and Fig. 11(d).

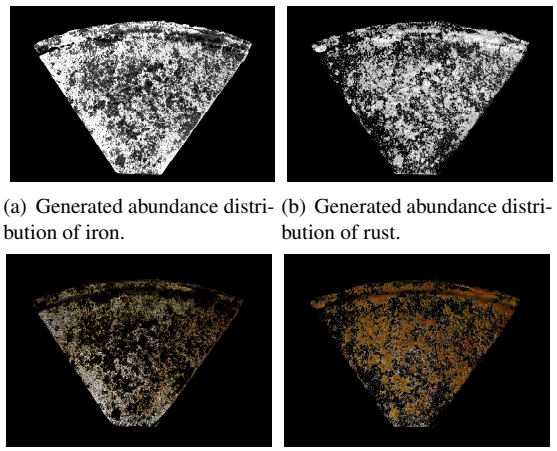

(a) Generated abundance distribution of iron. (b) Generated abundance distribution of rust.

(c) Areas with at least 60% iron. (d) Areas with at least 60% rust.

Figure 11: Linear unmixing results.

6 SUMMARY AND CONCLUSION

We have presented an approach for the acquisition and segmentation of spectral BRDF data. The data are recorded by relating object intensity data and reflectance standard data, which then directly provides BRDF measurements. We used those data to show that it is possible to obtain accurate segmentation results and endmember abundance estimates for objects with rapidly and with gradually changing materials, even if only a single light source position and a single viewpoint is available. The object surface with abrupt region boundaries has been classified with an accuracy of 88.5% (94.8% with some oversegmentation tolerance). The application of linear spectral unmixing to the separation of iron from rust for the gradually changing material has provided a qualitatively realistic result.

In summary, we thus note that it is possible to determine object regions correctly even if only a single light source and a single viewpoint are available, which is very important for e.g. industrial measurement setups. We have observed some limitation when using raw measured depth data, which has been found to be too noisy for correct incidence and viewing angle determination. This problem has been solved by using a model-based cylindrical and plane fit for the respective objects. Using laser range scanners with higher depth and lateral resolution can overcome that limitation easily.

The Phong and Cook-Torrance BRDF models were then fitted to the previously segmented cluster data. Due to the sparse data input (limited rage of incidence and viewing directions), some uncertainties in determining a hemispherical BRDF remain, especially for obliquely viewed surface parts. Additionally, the obtained BRDF tends to exhibit lower reflectance values for large observation angles $|\vartheta_o| \geq 60°$, which can be explained by a "diffuse fall-off" [DRS08]. This issue requires considerable attention in further research, since it requires a phenomenological (rather than empirical) adjustment of the reflectance model.

7 REFERENCES

[CM02] D. Comaniciu and P. Meer. Mean shift: A robust approach toward feature space analysis. *IEEE Transactions on Pattern Analysis and Machine Intelligence*, 24(5):603–619, 2002.

[CT81] R. L. Cook and K. E. Torrance. A reflectance model for computer graphics. *Proceedings of the 8th annual conference on Computer graphics and interactive techniques*, 15(3):307 – 316, 1981.

[DRS08] J. Dorsey, H. Rushmeier, and F. Sillion. *Digital Modeling of Material Appearance*. Morgan Kaufmann, 2008.

[Ebe08] D. Eberly. Fitting 3d data with a cylinder. *online* `http://www.geometrictools.com/Documentation/CylinderFitting.pdf`, 1:1–4, 2008.

[Fin06] B. Finkston. Mean Shift Clustering. *online* `http://www.mathworks.com/matlabcentral/fileexchange/10161-mean-shift-clustering`, 2006.

[HB86] B. K. P. Horn and Brooks. The variational approach to shape from shading. *Computer Vision, Graphics and Image Processing*, 33:174–208, 1986.

[HW12] S. Herbort and C. Wöhler. Self-consistent 3d surface reconstruction and reflectance model estimation of metallic surfaces. *VISAPP'2012*, pages 1–8, 2012.

[KM02] N. Keshava and J. F. Mustard. Spectral unmixing. *IEEE Signal Processing Magazine*, January 2002:44–57, 2002.

[LFTG97] E. P. F. Lafortune, S.-C. Foo, K. E. Torrance, and D. P. Greenberg. Non-linear approximation

 ISBN 978-80-86943-74-9

of reflectance functions. *SIGGRAPH'97*, pages 117–126, 1997.

[LHW12] M. Lenoch, S. Herbort, and C. Wöhler. Robust and accurate light source calibration using a diffuse spherical calibration object. *Oldenburger 3D Tage 2012*, 11:1–8, 2012.

[LKG+03] H. P. A. Lensch, J. Kautz, M. Goesele, W. Heidrich, and H.-P. Seidel. Image-based reconstruction of spatial appearance and geometric detail. *ACM Transactions on Graphics*, 22(2):234–257, 2003.

[LMM98] G. Lukacs, R. Martin, and D. Marshall. Faithful least-squares fitting of spheres, cylinders, cones and tori for reliable segmentation. *ECCV '98*, 1:671–686, 1998.

[Mar09] S. Marsland. *Machine Learning: An Algorithmic Perspective*. Chapman & Hall/CRC Machine, 2009.

[NRN03] S. G. Narasimhan, V. Ramesh, and S. K. Nayar. A class of photometric invariants: Separating material from shape and illumination. *Proceedings of the Ninth IEEE International Conference on Computer Vision - Volume 2*, pages 1387–, 2003.

[ON94] M. Oren and S. K. Nayar. Generalization of lambert's reflectance model. *Proceedings of the 21st Annual Conference on Computer Graphics and Interactive Techniques (SIGGRAPH 1994)*, pages 239–246, 1994.

[Pho75] B. T. Phong. Illumination for computer generated pictures. *Communications of the ACM*, 18(6):311–17, 1975.

[Sha85] S. A. Shafer. Using color to separate reflection components. *Color Research and Application*, 10(4):210–218, 1985.

[Tom02] S. Tominaga. Region segmentation by multispectral imaging. *Fifth IEEE Southwest Symposium on Image Analysis and Interpretation*, pages 238–242, 2002.

[Woo80] R. J. Woodham. Photometric method for determining surface orientation from multiple images. *Optical Engineering*, 19(1):139–144, 1980.

8 APPENDIX

Fig. 12 and Fig. 13 show image data for four exemplary wavelengths ($\lambda = 450\,\text{nm}, 550\,\text{nm}, 650\,\text{nm}, 750\,\text{nm}$). Note, that the pixels that correspond to a certain color / material have a designated intensity characteristic. The mean shift and *k*-means approaches described in the paper analyze that characteristic and group similar characteristics. It can be observed that e.g. rust has a lower 450 nm component than iron (i.e. less blue), but contains a more intense 650 nm and 750 nm component (more red). These relations exist over the whole dataset and thus allow the application of the unmixing approach.

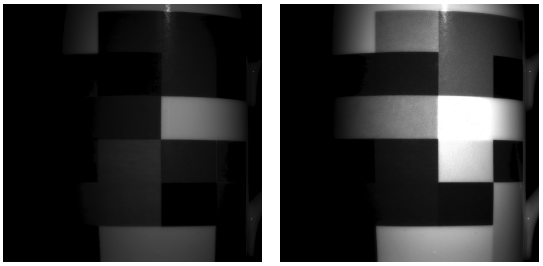

(a) 450nm (b) 550nm

(c) 650nm (d) 750nm

Figure 12: Camera image examples from the "cup" dataset. All images have been converted to the same reference intensity to facilitate image comparisons.

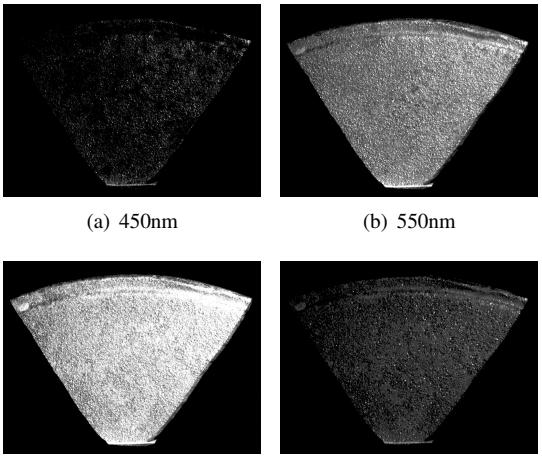

(a) 450nm (b) 550nm

(c) 650nm (d) 750nm

Figure 13: Camera image examples from the "triangle" dataset. All images have been converted to the same reference intensity to facilitate image comparisons.

 ISBN 978-80-86943-74-9